One-Dimensional Constrained Coulomb Structure Control with Charge Saturations

Shuquan Wang and Hanspeter Schaub

Abstract—A Coulomb structure is a cluster of free-flying satellites which maintains its shape through inter-vehicle electrostatic forces. These Coulomb forces are generated using on-board charge emission devices. This paper investigates the 1-D restricted motion of a 3-craft cluster. Two charge feedback strategies are discussed where the charge saturation limitation is considered. First a continuous formation shape feedback control strategy is presented. Next, a saturated control strategy is developed to arrest any relative velocities of the Coulomb structure. If the structure can be brought to rest, then the continuous charge control can be engaged to achieve the desired virtual structure. The saturated feedback control is developed using Lyapunov's direct method and can control the separation rates between the satellites by changing the signs of the three saturated charge products. Implementable real-charge solutions are ensured through scaling the Lyapunov function rate. The control is shown to be Lyapunov stable. Because of the limitations of the control charge magnitudes, certain initial conditions will not lead to the desired zero relative motion rates. Conditions under which the relative motion of the Coulomb structure can be stabilized are analyzed through investigating the total energy of the system in the symmetric motion assumption. The general convergence areas are illustrated numerically in various state planes. Simulations demonstrate the performance of the control.

I. INTRODUCTION

King et al. [1] originally discussed the novel method of exploiting Coulomb forces for formation flying in 2002. Since then many papers have been published in this area. Coulomb forces are proposed to control a tight formation with separation distances up to 100 meters. Electrostatic force fields are generated to control the formation's shape and size. Other promising techniques for close proximity flying include Electric Propulsion (EP) [1] and Electro-Magnetic Formation Flying (EMFF) [2]. EP systems generate forces by expelling ionic plumes. The ionic plumes can disturb the motions of nearby spacecraft. Further, the intensive and caustic charge plumes can also damage sensitive instruments. The EMFF method controls relative separation and attitude of the formation by creating electromagnetic dipoles on each spacecraft in concert with reaction wheels. In contrast to the EP method, the Coulomb formation flying technique has no exhausting plume contamination issues. The Coulomb force field in a vacuum is also simpler to model (point charge model) than the electromagnetic force field (dipole model), and the strength

only drops off with the square of the separation distance and not the qubic as with the electromagnetic force field. The generation of Coulomb forces has been shown to require only several watts of electric power; and can be controlled on a millisecond time scale [3]. In addition, Coulomb force control is 3-5 orders of magnitude more fuel-efficient than EP [1]. This is an essential advantage in long-term space missions.

Many challenges in Coulomb formation flying have been investigated. Joe et al. introduced a formation coordinate frame which tracks the principal axes of the formation in Reference 4. Parker et al. presented a sequential control strategy for arranging N charged bodies into an arbitrary geometry using $N + 3$ participating bodies in Reference 5. In this paper the authors overcame two challenging problems of Coulomb force control: the Coulomb force coupling and unimplementable control solutions that arise from the quadratic charge non-linearity. First-order differential orbit-element constraints for Coulomb formations are studied in Reference 6. Natarajan et al. developed charge feedback laws to stabilize the relative distance between two satellites of a Coulomb tether formation in References 7, 8 and 9. For the nadir-aligned 2 craft case the in-plane attitude of the Coulomb tether formation was stabilized by exploiting the gravity gradient torque. Hussein and Schaub studied shape-preserving Coulomb formations of three craft flying in deep space in Reference 10. They derived conditions that guaranteed preservation of the geometric shape of the formation. Schaub and Hussein in Reference 11 investigated the open-loop stable 2-craft Coulomb tether problem. They showed that the nonlinear radial motion was locally stable if the separation distance was less than the Debye length, and it was guaranteed to be unstable if the distance is larger than the Debye length. The same authors studied the stability and control of relative equilibria for the three-craft Coulomb tether problem in Reference 12.

This paper considers the control of a virtual Coulomb structure. A virtual Coulomb structure is composed of several spacecraft and the structure's shape and size are controlled by utilizing the inter-spacecraft electrostatic forces. This virtual structure control can be used in large scale distributed spacecraft concepts. The general three-dimensional charged spacecraft motion is very complex, and its control is an open area of research. This paper focuses on the 1-D restricted 3-craft Coulomb virtual structure to investigate charge implementability issues and charge saturation limitations. This control is directly applicable to the control of three charged test vehicles on a non-conducting hover track. Such a test bed is envisioned to perform basic charged vehicle relative motion control experiments. The craft are assumed to only experience

Shuquan Wang, Graduate Research Assistant, Aerospace Engineering Sciences Department, University of Colorado at Boulder, CO 80309

Hanspeter Schaub, Associate Professor, H. Joseph Smead Fellow, Aerospace Engineering Sciences Department, University of Colorado at Boulder, CO 80309

electrostatic forces. No orbital motion is modeled. The relative kinetic energy is investigated to provide bounds on the initial conditions to guarantee convergence in the presence of charge saturations.

Because of the limited amount of charge that a spacecraft can safely store, the Coulomb structure's shape may be uncontrollable in situations with large initial separation distances or large relative kinetic energy cases. For example, if the three spacecraft are departing each other at very high speeds, like meters' level comparing to centimeters' level speed that this paper is working with, then the limited actuation capability of the saturated Coulomb forces may not be able to pull them back to construct a virtual structure.

Noting this fact, this paper develops a two-stage control strategy. First a saturated control is engaged to arrest the relative motion of the spacecraft and stop its expansion. The magnitudes of the control charges are always kept at their maximum values, the only free variables are the signs of these control charges. In this control stage the controller explores the spacecraft's entire capability to arrest the relative motion in the formation. The failure of the saturated control implies that the spacecraft are flying too fast relative to the neighboring spacecraft in the formation to be controlled under current charge limits. Thus the domain where the saturated control can stabilize the relative motion is also the domain where the Coulomb formation can be controlled to certain desired shapes. The saturated control is designed using Lyapunov's direct method and the stability of this saturated control and the regions of convergence are investigated.

After the relative motion is stabilized, a continuous feedback law for formation shape control is employed to shape the structure to a certain desired configuration. This step completes the two-stage control strategy to control the shape of the 1-D constrained Coulomb structure with charge saturation limits. This 1-D constrained Coulomb structure control is a precursor for the more general study of the 3-D Coulomb structure control. It will also be implemented as the 1-D non-conducting hover track control test bed which is under construction in the Automatic Vehicle Control (AVS) Lab in the Aerospace Engineering Sciences department at the University of Colorado at Boulder.

II. CHARGED SPACECRAFT EQUATIONS OF MOTION

Let the Coulomb structure consist of 3 bodies with masses m_i which are restricted to move in only one dimension as illustrated in Figure 1. This setup simulates the motion of the test vehicles floating on a non-conducting hover track. The inertial positions of the three bodies are given through their inertial coordinates x_i. Without loss of generality, assume that $x_1 < x_2 < x_3$. Assume that the spacecraft are flying freely in space. In the scenario shown in Figure 1, assuming that the force acting from left to right to be positive, the inertial
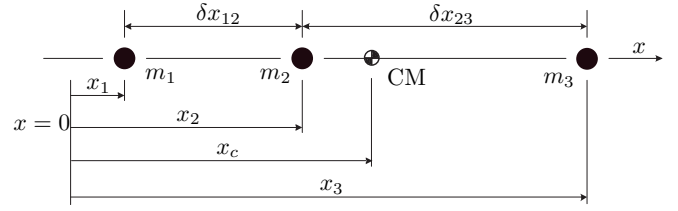

Fig. 1.   Illustration of 1-D constrained coordinates of the 3-body system.

equations of motion of the charged bodies are given by

$$m_1 \ddot{x}_1 = k_c \left[-\frac{Q_{12}}{(x_2 - x_1)^2} - \frac{Q_{13}}{(x_3 - x_1)^2} \right] \qquad (1)$$

$$m_2 \ddot{x}_2 = k_c \left[\frac{Q_{12}}{(x_2 - x_1)^2} - \frac{Q_{23}}{(x_3 - x_2)^2} \right] \qquad (2)$$

$$m_3 \ddot{x}_3 = k_c \left[\frac{Q_{13}}{(x_3 - x_1)^2} + \frac{Q_{23}}{(x_3 - x_2)^2} \right] \qquad (3)$$

where $k_c = 8.99 \times 10^9 \, \mathrm{C}^{-2} \cdot \mathrm{N} \cdot \mathrm{m}^2$ is the Coulomb constant, $Q_{ij} = q_i q_j$ is the charge product between the ith and j^{th} craft. This product is introduced here because the charges q_i always appear in pairs $q_i q_j$ both in the dynamic equation and in the control formulation. This approach leads to the problem of physical feasibility in extracting individual charges q_i from a given set of charge products Q_{ij}. This issue is addressed in the later sections. A charge feedback law is expected to control the relative motion of the three-body Coulomb structure and make the formation assume a specific shape defined through the separation distances.

Not all of the inertial x_i states can be controlled independently. Because the spacecraft charges produce formation internal forces, the momentum of the Coulomb cluster must be conserved if there are no other external forces acting on it. As a result it is not possible to independently control all three inertial coordinates x_i using only Coulomb forces. For the 1-D motion considered in this paper, the conservation of the linear momentum imposes one constraint on the generalized coordinates x_1, x_2 and x_3. Thus, the motion of the three-body system only has two controlled degrees of freedom (DOF). The formation shape is defined through the two separation distances δx_{12} and δx_{23} as:

$$\delta x_{12} = x_2 - x_1, \qquad \delta x_{23} = x_3 - x_2. \qquad (4)$$

The third distance δx_{13} is determined by $\delta x_{13} = \delta x_{12} + \delta x_{23}$. To control the shape of the Coulomb structure is to drive $[\delta x_{12}, \delta x_{23}]^T$ to the desired constant values $[\delta x_{12}^*, \delta x_{23}^*]^T$ that yield a specific virtual structure shape. For the control development, let the system state vector $\boldsymbol{X}$ be defined as the relative distance tracking error:

$$\boldsymbol{X} = \begin{bmatrix} \Delta x_{12} \\ \Delta x_{23} \end{bmatrix} = \begin{bmatrix} \delta x_{12} - \delta x_{12}^* \\ \delta x_{23} - \delta x_{23}^* \end{bmatrix}. \qquad (5)$$

This paper only considers the shape control of the Coulomb structure, and does not attempt to control the formation cluster's center of mass motion. From the inertial equations of motion in Eqs. (1)–(3), using the definition of δx_{ij}, the

separation distance equations of motion are found as

$$\delta\ddot{x}_{12} = \ddot{x}_2 - \ddot{x}_1 = k_c\left(\frac{1}{m_1} + \frac{1}{m_2}\right)\frac{Q_{12}}{\delta x_{12}^2} - \frac{k_c}{m_2}\frac{Q_{23}}{\delta x_{23}^2}$$
$$+ \frac{k_c}{m_1}\frac{Q_{13}}{\delta x_{13}^2}, \tag{6}$$

$$\delta\ddot{x}_{23} = \ddot{x}_3 - \ddot{x}_2 = -\frac{k_c}{m_2}\frac{Q_{12}}{\delta x_{12}^2} + k_c\left(\frac{1}{m_2} + \frac{1}{m_3}\right)\frac{Q_{23}}{\delta x_{23}^2}$$
$$+ \frac{k_c}{m_3}\frac{Q_{13}}{\delta x_{13}^2}, \tag{7}$$

The formation kinetic energy T is a convenient measure for constructing a Lyapunov function of the system and analyzing the stability of the equilibrium:

$$T = \frac{1}{2}\sum_{i=1}^{3} m_i \dot{x}_i^2. \tag{8}$$

However, the control goal is to let the virtual structure assume a certain shape, which implies that the relative kinetic energy should be zero. Thus the inertial kinetic energy expression in Eq. (8) needs to be rewritten in terms of the relative coordinate rates $\delta\dot{x}_{12}$ and $\delta\dot{x}_{23}$. Taking a time derivative of Eq. (4) yields

$$\dot{x}_1 = \dot{x}_2 - \delta\dot{x}_{12}, \qquad \dot{x}_3 = \dot{x}_2 + \delta\dot{x}_{23} \tag{9}$$

Substituting Eq. (9) into Eq. (8) leads to

$$T = \frac{M}{2}\dot{x}_2^2 + \frac{m_1}{2}\delta\dot{x}_{12}^2 + \frac{m_3}{2}\delta\dot{x}_{23}^2 + \dot{x}_2(m_3\delta\dot{x}_{23} - m_1\delta\dot{x}_{12}) \tag{10}$$

where $M = \sum_{i=1}^{3} m_i$ is the total mass of the three spacecraft cluster. The expression of the total kinetic energy in Eq. (10) still contains an inertial rate variable $\dot{x}_2$ which cannot be controlled independently with Coulomb forces. One more step to express $\dot{x}_2$ in terms of $\delta\dot{x}_{ij}$ is needed.

Note that the Coulomb forces are internal forces in the Coulomb structure, by the assumption mentioned at the beginning that the spacecraft are flying freely in deep space, the following center of mass condition must be true:

$$m_1\dot{x}_1 + m_2\dot{x}_2 + m_3\dot{x}_3 = M\dot{x}_c \tag{11}$$

where x_c is the inertial cluster center of mass coordinate. Utilizing Eq. (11), yields the following equation:

$$M\dot{x}_2 = M\dot{x}_2 - m_1\dot{x}_1 - m_2\dot{x}_2 - m_3\dot{x}_3 + M\dot{x}_c$$
$$= m_1\dot{x}_2 - m_1\dot{x}_1 + m_2\dot{x}_2 - m_2\dot{x}_2 + m_3\dot{x}_2$$
$$- m_3\dot{x}_3 + M\dot{x}_c$$
$$= m_1\delta\dot{x}_{12} - m_3\delta\dot{x}_{23} + M\dot{x}_c \tag{12}$$

Thus $\dot{x}_2$ is expressed in terms of δx_{ij} as:

$$\dot{x}_2 = \frac{1}{M}(m_1\delta\dot{x}_{12} - m_3\delta\dot{x}_{23}) + \dot{x}_c \tag{13}$$

Substituting Eq. (13) into Eq. (10), yields

$$T = \frac{1}{2}\dot{\boldsymbol{X}}^T[M]\dot{\boldsymbol{X}} + \frac{M}{2}\dot{x}_c^2 \tag{14}$$

where $[M]$ is the system mass matrix:

$$[M] = \frac{1}{M}\begin{bmatrix} m_1m_2 + m_1m_3 & m_1m_3 \\ m_1m_3 & m_1m_3 + m_2m_3 \end{bmatrix} \tag{15}$$

Obviously, $[M]$ is a positive definite matrix. Finally, the kinetic energy T_{rel} of the 3-craft cluster relative to the center of mass is given by

$$T_{\mathrm{rel}} = \frac{1}{2}\dot{\boldsymbol{X}}^T[M]\dot{\boldsymbol{X}} \tag{16}$$

This energy expression directly reflects whether the virtual structure shape is changing its geometry with time.

III. CONTROL STRATEGY

A. Shape Coordinate Equations of Motion

This section develops a continuous feedback control strategy that controls the 1-D 3-body formation to a certain desired shape. The desired shape is given by a vector of separation distances $[\delta x_{12}^*, \ \delta x_{23}^*]^T$, and it is assumed to be stationary (i.e. constant desired shape).

For notational convenience the 3×1 vector $\boldsymbol{\xi}$ is introduced as:

$$\boldsymbol{\xi} = \left[\frac{k_cQ_{12}}{\delta x_{12}^2}, \ \frac{k_cQ_{23}}{\delta x_{23}^2}, \ \frac{k_cQ_{13}}{\delta x_{13}^2}\right]^T = k_c[D]\boldsymbol{Q} \tag{17}$$

where $[D] = \mathrm{diag}\left(\frac{1}{\delta x_{12}^2}, \frac{1}{\delta x_{23}^2}, \frac{1}{\delta x_{13}^2}\right)$ is a diagonal matrix, $\boldsymbol{Q} = [Q_{12}, Q_{23}, Q_{13}]^T$ is a vector of the charge products. The vector $\boldsymbol{Q}$ is also the control input of the Coulomb structure control system. Because the desired relative position coordinates are constants, the tracking error dynamics is expressed using $\boldsymbol{X}$ as

$$\ddot{\boldsymbol{X}} = \underbrace{\begin{bmatrix} \frac{1}{m_1} + \frac{1}{m_2} & -\frac{1}{m_2} & \frac{1}{m_1} \\ -\frac{1}{m_2} & \frac{1}{m_2} + \frac{1}{m_3} & \frac{1}{m_3} \end{bmatrix}}_{[A]}\boldsymbol{\xi} = k_c[A][D]\boldsymbol{Q} \tag{18}$$

B. Formation Shape Control

The controller in this subsection is intended to make the formation attain a certain shape, which means both $\dot{\boldsymbol{X}}$ and $\boldsymbol{X}$ are driven to zero. For the time being the control development does not consider spacecraft charge saturation issues.

1) Minimum Norm Shape Stabilizing Control: Because the state vector $\boldsymbol{X}$ and the time derivative of the state vector $\dot{\boldsymbol{X}}$ are all expected to be zero, the Lyapunov function candidate here is defined as a quadratic function of $\boldsymbol{X}$ and $\dot{\boldsymbol{X}}$ as

$$V_1 = \frac{1}{2}\dot{\boldsymbol{X}}^T[M]\dot{\boldsymbol{X}} + \frac{1}{2}\boldsymbol{X}^T[K]\boldsymbol{X} \tag{19}$$

where $[K]$ is a 2×2 positive definite matrix. Because both $[M]$ and $[K]$ are positive definite, V_1 is a positive definite function of $\dot{\boldsymbol{X}}$ and $\boldsymbol{X}$. Note that the first term in V_1 is the relative kinetic energy T_{rel} of the system.

Differentiating Eq. (19) with respect to time, and utilizing the shape error equations of motion in Eq. (18), yields

$$\dot{V}_1 = \dot{\boldsymbol{X}}^T[K]\boldsymbol{X} + \dot{\boldsymbol{X}}^T[M]\ddot{\boldsymbol{X}} = \dot{\boldsymbol{X}}^T\left([K]\boldsymbol{X} + [M][A]\boldsymbol{\xi}\right) \tag{20}$$

Denote $[C] = [M][A]$; it turns out to be a constant matrix with the following simple form:

$$[C] = \begin{bmatrix} 1 & 0 & 1 \\ 0 & 1 & 1 \end{bmatrix} \tag{21}$$

Next the Lyapunov function rate $\dot{V}_1$ is set to the negative semi-definite form

$$\dot{V}_1 = -\dot{\boldsymbol{X}}^T[P]\dot{\boldsymbol{X}} \tag{22}$$

where $[P]$ is a 2×2 positive definite matrix. $\dot{V}_1$ is negative semi-definite because $\dot{V}_1$ is a function of both $\dot{\boldsymbol{X}}$ and $\boldsymbol{X}$, but only $\dot{\boldsymbol{X}}$ appears in Eq. (22).

Equating the actual $\dot{V}_1$ in Eq. (20) and the desired $\dot{V}_1$ in Eq. (22) leads to the following feedback control condition:

$$[C]\boldsymbol{\xi} = -[K]\boldsymbol{X} - [P]\dot{\boldsymbol{X}} \tag{23}$$

Solving Eq. (23) for $\boldsymbol{\xi}$ yields the charge product vector that stabilizes the system. Because $[C]$ only has rank 2, there is an infinite number of solutions for $\boldsymbol{\xi}$ in Eq. (23). Let $\hat{\boldsymbol{\xi}}$ be the minimum norm solution to Eq. (23):

$$\hat{\boldsymbol{\xi}} = -[C]^{\dagger}\left([K]\boldsymbol{X} + [P]\dot{\boldsymbol{X}}\right) \tag{24}$$

where $[C]^{\dagger} = [C]^T([C][C]^T)^{-1}$ is the minimum norm pseudo-inverse of matrix $[C]$. The hat symbol above the vector $\boldsymbol{\xi}$ means that $\hat{\boldsymbol{\xi}}$ given by Eq. (24) is the minimum norm solution among the general solutions to Eq. (23); and $\hat{\boldsymbol{\xi}}$ is not the final solution of $\boldsymbol{\xi}$ that will be used in the control. Note that $\hat{\boldsymbol{\xi}}$ in Eq. (24) minimizes the norm of the charge product vector while satisfying Eq. (23), but not the charge inputs q_i of the control.

2) Spacecraft Charge Computation Issues: After obtaining a solution $\boldsymbol{\xi}$ to Eq. (23), the charge product vector is given by

$$\boldsymbol{Q} = \frac{1}{k_c}[D]^{-1}\boldsymbol{\xi} \tag{25}$$

The individual charges q_i are finally calculated through the algorithm [13]

$$q_1 = \sqrt{\frac{Q_{12}Q_{13}}{Q_{23}}} \tag{26a}$$

$$q_2 = \text{sign}(Q_{12})\frac{Q_{12}}{q_1} \tag{26b}$$

$$q_3 = \text{sign}(Q_{13})\frac{Q_{13}}{q_1} \tag{26c}$$

Note that a singularity occurs if $\xi_1 \cdot \xi_2 \cdot \xi_3 = 0$. When one or two elements of $\boldsymbol{\xi}$ equal zero, this singularity can be avoided by performing a search routine in the null space of the $[C]$ matrix which will be discussed in the following several paragraphs. The remaining case is that $\boldsymbol{\xi} = \boldsymbol{0}$ which indicates that $q_1 = q_2 = q_3 = 0$. This state occurs only either when $\boldsymbol{X} = 0$ and $\dot{\boldsymbol{X}} = 0$, which means the system has reached the desired state, or due to $(-[K]\boldsymbol{X} - [P]\dot{\boldsymbol{X}})$ being zero.

Now consider general cases where $\xi_1 \cdot \xi_2 \cdot \xi_3 \neq 0$. Note that $\xi_1 \cdot \xi_2 \cdot \xi_3 < 0$ yields imaginary values of q_i [13]. Since charges must always be real numbers, $\xi_1 \cdot \xi_2 \cdot \xi_3 < 0$ is not an implementable solution. This is a fundamental issue with developing any charge feedback law.

Eq. (24) provides the minimum norm solution $\hat{\boldsymbol{\xi}}$ of $\boldsymbol{\xi}$ to Eq. (23). There is an infinite number of solutions that satisfy Eq. (23) since the matrix $[C]$ is a 2×3 matrix. Using the null

space of $[C]$, all possible $\boldsymbol{\xi}$ values that satisfy Eq. (23) are parameterized as

$$\boldsymbol{\xi} = \begin{pmatrix} \xi_1 \\ \xi_2 \\ \xi_3 \end{pmatrix} = \hat{\boldsymbol{\xi}} + \gamma \begin{pmatrix} -1 \\ -1 \\ 1 \end{pmatrix} \tag{27}$$

where the parameter γ can be any real number. The control problem is reformulated to determine a parameter γ that satisfies the implementability constraint:

$$f(\gamma) = \xi_1 \cdot \xi_2 \cdot \xi_3 = (\hat{\xi}_1 - \gamma)(\hat{\xi}_2 - \gamma)(\hat{\xi}_3 + \gamma) > 0 \tag{28}$$

This inequality constraint guarantees that the charges q_i are real, and also ensures that the singularity case $\xi_1 \cdot \xi_2 \cdot \xi_3 = 0$ does not occur. Because $f(\gamma)$ is a third order function, there always exists real numbers of parameter γ that satisfy the inequality in Eq. (28).

3) Charge Minimization Routine: Any real value of parameter γ that satisfies the inequality in Eq. (28) makes the solution physically implementable with real charge q_i solutions. In fact, the null space of the input matrix $[C]$ can be used to charge up the vehicles without causing any relative motion to occur. The $\hat{\boldsymbol{\xi}}$ vector is found such that the norm of the vector $\boldsymbol{\xi}$ is minimized. However, this doesn't correspond to the solution that the spacecraft charges q_i are minimized. Define a charge cost function $J(\gamma)$ as

$$J(\gamma) = \sum_{i=1}^{3} q_i^2 \tag{29}$$

The solution $\boldsymbol{\xi}$ that minimizes spacecraft charges q_i corresponds to a particular γ_m that satisfies the inequality constraint in Eq. (28), and at the same time minimizes the charge cost function $J(\gamma)$.

Consider the constraint inequality in Eq. (28), where $(\hat{\xi}_1, \hat{\xi}_2, \hat{\xi}_3)$ are given by Eq. (24). There are three real roots for the equation $f(\gamma) = 0$ which are $(\hat{\xi}_1, \hat{\xi}_2, -\hat{\xi}_3)$. We rearrange the roots in a descending order and denote them as $(\gamma_1, \gamma_2, \gamma_3)$, where $\gamma_1 \geq \gamma_2 \geq \gamma_3$. The solution to the constraint in Eq. (28) turns out to be $\gamma > \gamma_1$ or $\gamma_3 < \gamma < \gamma_2$. If $\gamma_2 = \gamma_3$, then the solution is simply $\gamma > \gamma_1$. Figure 2(a) shows a numerical example of $f(\gamma)$ and $(\gamma_1, \gamma_2, \gamma_3)$.

Thus a charge minimizing routine is introduced to search for the parameter γ_m within the two open intervals (γ_1, ∞) and (γ_3, γ_2). The numerical search algorithm used in this paper is the secant method shown in Figure 3.

Once γ_m is obtained, the solution that minimizes the norm of the charge vector (q_1, q_2, q_3) is achieved, and of course it's also implementable. Figure 2 shows an example of the search result at one instant, where γ_{m1} and γ_{m2} are two local minimization points.

Notice that generally there are two eligible intervals in the search routine. Sometimes this may introduce chatter because γ_m switches between γ_{m1} and γ_{m2} when $J(\gamma_{m1})$ and $J(\gamma_{m2})$ are very close. To reduce the chatter of the charge history, one approach is to change the criteria for γ_m to switch between the two intervals. If $\gamma_m(i) = \gamma_{m1}(i)$, then $\gamma_m(i+1) = \gamma_{m2}(i+1)$ if and only if $J(\gamma_{m2}) < \alpha J(\gamma_{m1})$, where $0 < \alpha \leq 1$. Or in words, the charge solutions are only switched to the alternate set if the change in the cost function is sufficiently large.
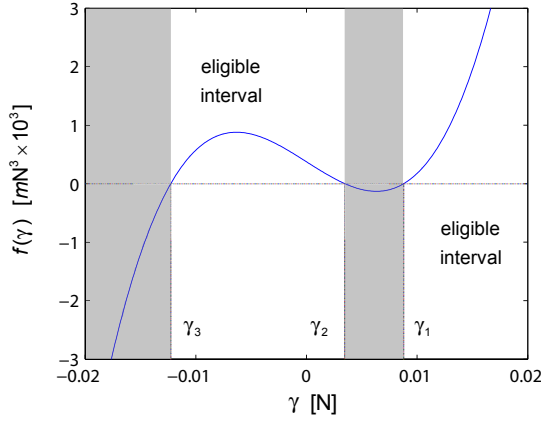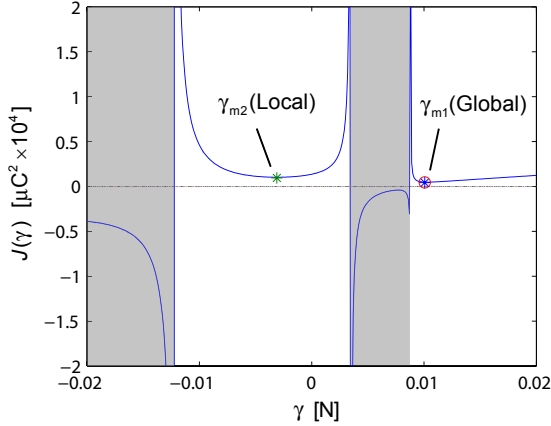
(a) $f(\gamma)$ and $(\gamma_1, \gamma_2, \gamma_3)$.

(b) γ_m search result.

Fig. 2.   Illustration of γ_m search routine.

C. Formation Shape Rate Regulation

This subsection develops a regulator that arrests the relative motion of the formation by driving $\dot{\boldsymbol{X}}$ to zero. After presenting a saturated stabilizing control strategy, a method to obtain implementable spacecraft charges q_i is introduced.

1) Saturated Regulator: Because the purpose of the control is different from that of the shape control presented in section III-B, a new Lyapunov function is introduced catering to the new demand. The regulator is intended to stop any relative motion of the formation, so the new Lyapunov function candidate V_2 is defined in terms of the relative velocity vector in a quadratic, positive definite form:

$$V_2 = T_{\text{rel}} = \frac{1}{2} \dot{\boldsymbol{X}}^T [M] \dot{\boldsymbol{X}} \qquad (30)$$

Taking time derivative of V_2, and using the tracking error dynamics in Eq. (18), yields

$$\dot{V}_2 = \dot{\boldsymbol{X}}^T [M] \ddot{\boldsymbol{X}} = k_c \dot{\boldsymbol{X}}^T [C][D] \boldsymbol{Q} \qquad (31)$$

The saturated control strategy attempts to drive the rates $\dot{\boldsymbol{X}}$ to zero as quickly as possible, leading to a Lyapunov optimal control development [14]. Here the spacecraft charges are always held at the maximum magnitude. The control algorithm
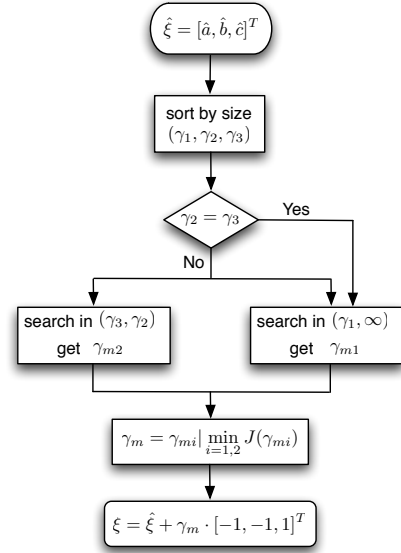
Fig. 3.   Illustration of γ_m search routine.

will need to determine the required signs of the spacecraft charges. The charge product vector $\boldsymbol{Q}$ is expressed as

$$\boldsymbol{Q} = \begin{bmatrix} Q_{12m} & 0 & 0 \\ 0 & Q_{23m} & 0 \\ 0 & 0 & Q_{13m} \end{bmatrix} \begin{bmatrix} s_1 \\ s_2 \\ s_3 \end{bmatrix} = [Q_m] \boldsymbol{s} \qquad (32)$$

where $Q_{ijm} = q_{im} q_{jm}$ is the product of the charge saturation limits of the ith and j^{th} spacecraft. The vector $\boldsymbol{s} = \text{sign}(\boldsymbol{Q})$ is a 3×1 sign vector with the components being ± 1 or zero. The matrix $[Q_m]$ is a constant matrix determined by charge limitations of the spacecraft. Because $[Q_m]$ is constant for a given 3-body Coulomb structure, the charge product $\boldsymbol{Q}$ is determined only by $\boldsymbol{s}$. Thus the vector $\boldsymbol{s}$ is actually the essential variable that determines the saturated regulator. The Lyapunov function rate is rewritten as

$$\dot{V}_2 = k_c \dot{\boldsymbol{X}}^T [C][D][Q_m] \boldsymbol{s} \qquad (33)$$

To guarantee stability, the Lyapunov rate function $\dot{V}$ is set to be a negative semi definite function as

$$\dot{V}_2 = -\dot{\boldsymbol{X}}^T [P] \dot{\boldsymbol{X}} \qquad (34)$$

where $[P]$ is a 2×2 positive matrix. Note that Eq. (34) has the same form as Eq. (22).

Substituting Eq. (34) into Eq. (33) provides an equation to solve for $\boldsymbol{s}$. At first, let us treat $\boldsymbol{s}$ as a general vector instead of a sign vector. A sign vector can be obtained by evaluating the signs of the elements in $\boldsymbol{s}$. Note that $[C]$ is a 2×3 matrix, thus there is an infinite number of solutions for $\boldsymbol{s}$ after equating Eq. (34) and Eq. (33). Using the pseudo-inverse of matrix $[C]$, leads to the minimum norm solution $\tilde{\boldsymbol{s}}$ (the tilde symbol means $\tilde{\boldsymbol{s}}$ is not a sign vector) :

$$\tilde{\boldsymbol{s}} = -\frac{1}{k_c} [Q_m]^{-1} [D]^{-1} [C]^{\dagger} [P] \dot{\boldsymbol{X}} \qquad (35)$$

Define a sign vector s as:

$$s = \text{sign}(\tilde{s}) = -\text{sign}\left(\frac{1}{k_c}[Q_m]^{-1}[D]^{-1}[C]^\dagger[P]\dot{X}\right) \quad (36)$$

Here s is a sign vector, but it may be un-implementable. This problem will be discussed following this subsection. Substituting s in Eq. (36) into charge vector Q in Eq. (32) constructs a saturated charge product control law:

$$Q = [Q_m]s = -[Q_m]\text{sign}\left(\frac{1}{k_c}[Q_m]^{-1}[D]^{-1}[C]^\dagger[P]\dot{X}\right). \quad (37)$$

The resulting actual Lyapunov function rate should be investigated, because after taking the sign function of $\tilde{s}$, the actual Lyapunov function rate is different from the nominal one in Eq. (34). Substituting the actual charge product in Eq. (32) into Eq. (31), yields

$$\dot{V}_2 = k_c\dot{X}^T[C][D][Q_m]s = k_c\dot{X}^T[C][D][Q_m]\text{sign}(\tilde{s}) \quad (38)$$

Note that the sign function can be deemed as a rescaling of the magnitude of a number, a scale matrix is introduced:

$$[E] = \text{diag}(a_1, a_2, a_3), \quad (39)$$

where a_i is defined as

$$a_i = \begin{cases} \frac{1}{\|\tilde{s}_i\|}, & \text{if } \tilde{s}_i \neq 0 \\ 0, & \text{if } \tilde{s}_i = 0 \end{cases}. \quad (40)$$

Thus s can be rewritten as

$$s = [E]\tilde{s}. \quad (41)$$

Substituting Eq. (41) into Eq. (38), and using Eq. (35) yields

$$\begin{aligned} \dot{V}_2 &= k_c\dot{X}^T[C][D][Q_m][E]\tilde{s} \\ &= -\dot{X}^T\underbrace{[C][D][Q_m][E][Q_m]^{-1}[D]^{-1}[C]^\dagger[P]}_{[F]}\dot{X} \quad (42) \end{aligned}$$

Without loss of generality, set the positive definite matrix $[P]$ introduced in Eq. (34) to be a diagonal matrix:

$$[P] = \begin{bmatrix} p_1 & 0 \\ 0 & p_2 \end{bmatrix} \quad (43)$$

Utilizing previous definitions of matrices $[C]$, $[D]$, $[Q_m]$, $[E]$, and $[P]$, the matrix $[F]$ is expanded as:

$$[F] = \frac{1}{3}\begin{bmatrix} p_1(2a_1 + a_3) & p_2(-a_1 + a_3) \\ p_1(-a_2 + a_3) & p_2(2a_2 + a_3) \end{bmatrix} \quad (44)$$

From the condition $p_i > 0$, it can be verified that the matrix $[F]$ is positive definite if $a_i > 0$ and it is positive semi definite if $a_i \geq 0$. By the definition of matrix $[E]$, $a_i \geq 0$. So the matrix $[F]$ is positive semi definite. The sign of the actual Lyapunov function rate is then determined:

$$\dot{V}_2 = -\dot{X}^T[F]\dot{X} \leq 0. \quad (45)$$

Thus the saturated control law in Eq. (36) is globally stable. But it's not asymptotically stable because the matrix $[F]$ can be zero if the states X grow infinitely large.

2) Implementable Saturated Control: The saturated charge product control in Eq. (37) provides a globally stable control that stops the relative motion of the formation. But this formula doesn't ensure physical implementability of the charge products. Similar to the shape controller's design, an implementable sign vector $s = [s_1, s_2, s_3]$ must satisfy:

$$s_1 \cdot s_2 \cdot s_3 > 0 \quad (46)$$

Unlike the case in the shape control design, the saturated regulator should be dealt with care because the sign function (or the matrix $[E]$) scales everything inside its argument. Note that the matrix $[E]$ is also varying with its argument. The previous approach that explores the null space of a certain matrix doesn't easily work out because of the rescaling of the matrix $[E]$, and the coupling of the matrix $[E]$ with the sign function's argument.

Note that in designing the stabilizing saturated control using Lyapunov stability theory, the stability property is achieved by setting the Lyapunov function rate to be negative semi-definite. This is ensured by the positive-definite property of the 2×2 matrix $[P]$. In most cases, this matrix is constant because usually it's unnecessary to change the value of the matrix $[P]$ and a constant $[P]$ matrix may result in a better convergence property of the system. Because the saturated control in Eq. (37) is globally stable but not asymptotically stable, changing the matrix $[P]$ won't sacrifice convergence property of the system. Since the matrix $[P]$ is only required to be positive-definite to guarantee the stability of the system, there exists a flexibility in choosing $[P]$.

Without loss of generality, set the matrix $[P]$ to be diagonal: $[P] = \text{diag}(p_1, p_2)$. For $[P]$ to be positive-definite, the parameters p_1 and p_2 must be positive. Let p_1 and p_2 be constants. To set up a varying matrix $[P]$, a variable parameter τ is introduced to rewrite the matrix $[P]$ as

$$[P] = \begin{bmatrix} p_1 & 0 \\ 0 & \tau p_2 \end{bmatrix} \quad (47)$$

here $\tau > 0$ should be positive to ensure $[P]$ to be positive-definite. Note that because the matrices $[Q_m]$ and $[D]$ are all positive definite and diagonal, the sign vector in Eq. (36) can be simplified as

$$s = -\text{sign}([C]^\dagger[P]\dot{X}) \quad (48)$$

Substituting the values of the matrices $[C]^\dagger$ and $[P]$ into Eq. (48), the vector s is expanded as

$$s = -\text{sign}\left(\frac{1}{3}\begin{bmatrix} 2p_1\dot{x}_{12} - \tau p_2\dot{x}_{23} \\ -p_1\dot{x}_{12} + 2\tau p_2\dot{x}_{23} \\ p_1\dot{x}_{12} + \tau p_2\dot{x}_{23} \end{bmatrix}\right) \quad (49)$$

For the sign vector s to result in an implementable control, the vector inside the sign function must satisfy

$$(2p_1\dot{x}_{12} - \tau p_2\dot{x}_{23})(-p_1\dot{x}_{12} + 2\tau p_2\dot{x}_{23})(p_1\dot{x}_{12} + \tau p_2\dot{x}_{23}) < 0 \quad (50)$$

transform the inequality in Eq. (50) to be:

$$\begin{aligned} g(\tau) &= (p_2\dot{x}_{23}\tau - 2p_1\dot{x}_{12})(2p_2\dot{x}_{23}\tau - p_1\dot{x}_{12}) \\ &\quad \cdot(p_2\dot{x}_{23}\tau + p_1\dot{x}_{12}) > 0 \quad (51) \end{aligned}$$

Now the logic is clear that to find an implementable control by varying the matrix $[P]$ is to find a parameter $\tau > 0$ that satisfies the inequality $g(\tau) > 0$. Next the existence of a solution is verified. When $\dot{x}_{23} > 0$, the inequality in Eq. (51) can be transformed to

$$h(\tau) = \left(\tau - \underbrace{\frac{2p_1\dot{x}_{12}}{p_2\dot{x}_{23}}}_{b_1}\right)\left(\tau - \underbrace{\frac{p_1\dot{x}_{12}}{2p_2\dot{x}_{23}}}_{b_2}\right)\left(\tau + \underbrace{\frac{p_1\dot{x}_{12}}{p_2\dot{x}_{23}}}_{-b_3}\right) > 0 \tag{52}$$

Note that $h(\tau) \to \infty$ as $\tau \to \infty$. There always exists $\tau > 0$ such that $h(\tau) > 0$.

If $\dot{x}_{23} < 0$, the inequality in Eq. (52) changes to be

$$h(\tau) < 0 \tag{53}$$

Note that (b_1, b_2, b_3) are the three roots to the equation $h(\tau) = 0$, and they share the simple relation $\text{sign}(b_1) = \text{sign}(b_2) = -\text{sign}(b_3)$. When $b_1, b_2 > 0$ and $b_3 < 0$, then any $\tau \in (b_2, b_1)$ satisfies $h(\tau) < 0$. If $b_1, b_2 < 0$ and $b_3 > 0$, in this case any $\tau \in (0, b_3)$ satisfies $h(\tau) < 0$.

Note that $\dot{x}_{12} = 0$ or $\dot{x}_{23} = 0$ are transient states, unless $\dot{X} = 0$ which means the relative motion has been arrested. Thus there always exists $\tau > 0$ that results in an implementable control.

IV. DOMAINS OF CONVERGENCE

So far a two-stage control strategy has been presented to control the 1-D Coulomb formation. At first a saturated charge control is used to stop the relative motion of the 3 spacecraft. After the relative motion converges to zero, the formation shape control is activated to make the spacecraft to form a certain shape defined by the provided distances.

As mentioned before, the saturated charge control in Eq. (37) is globally stable, but not asymptotically stable. Under some initial conditions, such as the three spacecraft flying apart too fast, the relative motion cannot be arrested. This section is going to determine the domains of the initial conditions that result in stabilizable motions.

A. Convergence Criterion For Symmetric Relative Motion

In setting up experiments on hover track test bed, it's needed to know whether a configuration of the 1-D Coulomb structure can be stabilized. This section tries to find analytical conditions for stabilizable symmetric motions. Even though the symmetric motion is a special case for the 1-D Coulomb formation, it can be implemented in the hover track test bed.

Here the phrase "symmetric relative motion" means the distances between any two adjacent spacecraft are always equal to each other, and the adjacent distance rates are also equal. That is

$$\delta x_{12} = \delta x_{23}, \quad \delta \dot{x}_{12} = \delta \dot{x}_{23} \tag{54}$$

Corresponding to this situation, the masses and charge limits of each body should all be equal, $m_1 = m_2 = m_3 = m$, $q_{1\max} = q_{2\max} = q_{3\max} = q_{\max}$. In this case the description of the motion can be greatly simplified. This simplified case will

provide analytical insight into the specific instance when the saturated charge control is able to arrest any relative expansion.

For the 1-D Coulomb formation, the most likely scenario which could result in an unarrestable motion is that three spacecraft are departing from each other. That is $\delta \dot{x}_{12} > 0$ and $\delta \dot{x}_{23} > 0$. The following discussion deals with this "worst" case to find the criterion for the arrestable motions. The unarrestable motion happens when the center spacecraft attracts the two other spacecraft, but the distance rate vector $\dot{X}$ still doesn't decrease to zero. In this case the charges of the 3 spacecraft are

$$q_1 = q_3 = \pm q_{\max}, \quad q_2 = \mp q_{\max} \tag{55}$$

Reference 15 presents an analytical way to find the criteria for the avoidance of a potential collision between 2 charged craft. It assumes that the charge product is constant, thus the trajectory of the 2-body motion is a conic section. Utilizing the methodology from the gravitational 2-body problem (2BP), the criteria is found through calculating the periapsis radius which is the closest distance between the 2 spacecraft in the conic section trajectory.

Motivated by this analytical approach to solve the 2-body Coulomb forced motion, another concept from the traditional gravitational 2BP, total energy level, is introduced to study the 3-body 1-D Coulomb formation. Note that in the gravitational 2BP, the hyperbola is a non-retrievable trajectory type, and it corresponds to an energy level that is greater than zero. By assuming that the charges of the spacecraft are constant, the total energy (kinetic energy and potential energy) of the 3-body system is constant. The unarrestable motion corresponds to a positive energy level, and the stabilizable motion has a total energy that is negative.

The general relative kinetic energy T_{rel} is given by Eq. (16). Using the symmetric conditions provided above, T_{rel} is simplified to be

$$T_{\text{rel}} = \frac{m^2}{2M}\delta\dot{x}_{12}^2 + \frac{m^2}{2M}(\delta\dot{x}_{12} + \delta\dot{x}_{23})^2 + \frac{m^2}{2M}\delta\dot{x}_{23}^2 = \frac{M}{3}\delta\dot{x}_{12}^2 \tag{56}$$

where $M = 3m$ is the total formation mass. The electrostatic potential energy of the formation is

$$V_e = k_c\frac{Q_{12}}{\delta x_{12}} + k_c\frac{Q_{23}}{\delta x_{23}} + k_c\frac{Q_{13}}{\delta x_{12} + \delta x_{23}} \tag{57}$$

Utilizing the symmetric motion condition in Eq. (54) and Eq. (55), V_e is simplified to be

$$V_e = k_c\left(-\frac{q_{\max}^2}{\delta x_{12}} - \frac{q_{\max}^2}{\delta x_{12}} + \frac{q_{\max}^2}{2\delta x_{12}}\right) = -\frac{3k_cq_{\max}^2}{2\delta x_{12}} \tag{58}$$

Thus the total energy is obtained by adding up the kinetic energy and potential energy:

$$E_t = T_{\text{rel}} + V_e = \frac{M}{3}\delta\dot{x}_{12}^2 - \frac{3k_cq_{\max}^2}{2\delta x_{12}} \tag{59}$$

which has a very simple form due to the symmetric relative motion assumption. Because the charges of the spacecraft are constants in this saturated control discussion, the total energy

is also constant. For a stabilizable motion, the total energy E_t should be negative, that is

$$E_t = \frac{M}{3}\delta\dot{x}_{12}^2 - \frac{3k_c q_{max}^2}{2\delta x_{12}} < 0 \qquad (60)$$

If $E_t < 0$, then it is impossible for $\delta x_{12} \to \infty$. However, if $E_t > 0$, then $\delta\dot{x}_{12}$ will approach a positive value as $\delta x_{12} \to \infty$. Transforming Eq. (60) such that only δx_{12} and $\delta\dot{x}_{12}$ remain on the left hand side yields the condition

$$\delta\dot{x}_{12}^2\delta x_{12} < \frac{9k_c q_{max}^2}{2M} = \frac{3k_c q_{max}^2}{2m} \qquad (61)$$

Eq. (61) provides an analytical criterion for the initial states δx_{12} and $\delta\dot{x}_{12}$ to result in a stabilizable symmetric motion. From this criterion it can be seen that when the charges and masses of the three spacecraft are set, both the distance and distance rate should be within a certain range to ensure that the symmetric relative motion can be stopped. A bigger charge limit results in a bigger value in the right hand side of the inequality in Eq. (61). Thus the area in the $\delta x_{12} - \delta\dot{x}_{12}$ plane that satisfies the criterion is bigger. Note that this criterion is valid only for the symmetric relative motion of the 1-D Coulomb formation. The following discussion will investigate the convergence area of general motions of the 1-D Coulomb formation.

B. Convergence Area For General Cases

The previous subsection derives the converge criterion for the symmetric relative motion by investigating the total energy of the system. Due to the changing polarity of the spacecraft charges, the energy of the system is not constant even though the magnitude of the charges remain the same. It's very difficult to apply the similar approach as in the symmetric motion to analyze the general convergence area of the saturated control.

Though an analytical solution is difficult to achieve, numerical results are always obtainable. The convergence area can be illustrated by marking each set of initial conditions with which the distance rates converge to zeros in the numerical simulation. Without the assumption of symmetric motion, the initial conditions of the motion contain four independant variables: $[\delta x_{12}, \delta x_{23}, \delta\dot{x}_{12}, \delta\dot{x}_{23}]$. Thus the convergence area should be configured as a four dimensional region. To illustrate the convergences areas in 2-dimensional plots, the distances and distance rates are illustrated separately. After a certain set of initial $[\delta\dot{x}_{12}, \delta\dot{x}_{23}]$ is prescribed, the resulting initial $[\delta x_{12}, \delta x_{23}]$ conditions' area of convergence is illustrated in a 2-D phase plane. And the convergence area of the variables $[\delta\dot{x}_{12}, \delta\dot{x}_{23}]$ is demonstrated in the similar way in the $\delta\dot{x}_{12} - \delta\dot{x}_{23}$ plane.

Taking the 1-D non-conducting hover track vehicles as an example, let the masses be $m_1 = m_2 = m_3 = 10$kg, and the charge limits be $q_{1max} = q_{2max} = q_{3max} = q_{max} = 5 \times 10^{-5}$C. Let the control parameters be $p_1 = p_2 = 1$kg/(C²·s). Figure 4 shows the convergence areas of the distances $\delta x_{12}, \delta x_{23}$ under different initial distance rates. Figure 4(a) shows the case when the initial distance rates $[\delta\dot{x}_{12}, \delta\dot{x}_{23}] = [0.1, 0.1]$m/s. The shaded area represents the initial conditions which lead to
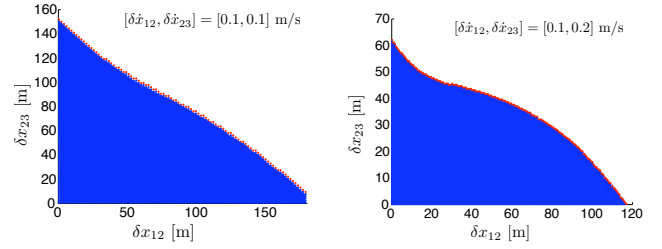
(a) $(\delta\dot{x}_{12}, \delta\dot{x}_{23}) = (0.1, 0.1)$m/s.   (b) $(\delta\dot{x}_{12}, \delta\dot{x}_{23}) = (0.1, 0.2)$m/s.

Fig. 4.   Area of convergence of $(\delta x_{12}, \delta x_{23})$.

converged states. It can be seen that the convergence area is not quite symmetric in δx_{12} and δx_{23} directions. This is because the charge implementation strategy by varying the matrix $[P]$ doesn't result in symmetric solutions while switching the values of the individual distances δx_{12} and δx_{23}. Figure 4(b) shows the convergence area of the $\delta x_{12} - \delta x_{23}$ plane when the initial distance rates are set to be $[\delta\dot{x}_{12}, \delta\dot{x}_{23}] = [0.1, 0.2]$m/s. The convergence area shrinks greatly in δx_{23} direction. This is because the departing speed $\delta\dot{x}_{23}$ is larger than $\delta\dot{x}_{12}$; it makes $\delta\dot{x}_{23}$ converge much more difficult than $\delta\dot{x}_{12}$.
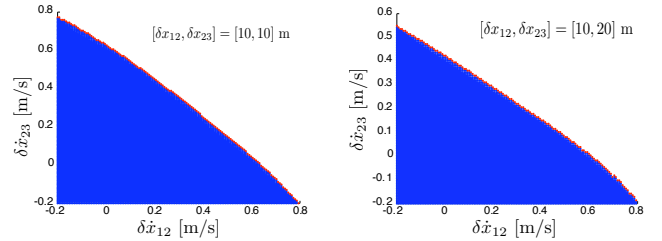
(a) $(\delta x_{12}, \delta x_{23}) = (10, 10)$m.   (b) $(\delta x_{12}, \delta x_{23}) = (10, 20)$m.

Fig. 5.   Area of convergence of $(\delta\dot{x}_{12}, \delta\dot{x}_{23})$.

Figure 5 illustrates two convergence areas of the distance rates in the $\delta\dot{x}_{12} - \delta\dot{x}_{23}$ plane. It can be seen that the convergence area reduces in the direction where the distance increases. The scales of the axes $\delta\dot{x}_{ij}$ range within $[-0.2, 0.8]$m/s in the plots. The negative distance rate means the two spacecraft are approaching each other. If the magnitude of the negative distance rate is too big, then the spacecraft are getting close too fast, this may result in collision of spacecraft which is not contained in the scope of this paper. Reference 15 develops the analytical criteria for two spacecraft which are approaching each other to be able to avoid a collision.

V. NUMERICAL SIMULATION

A two-stage control strategy has been developed to control the shape of the 1-D constrained Coulomb structure. At first the saturated control is used to arrest the relative motion of the spacecraft. After the relative motion has been stabilized, the formation shape controller is employed to make the formation construct a certain shape that is defined by the given desired distances $[\delta x_{12}^*, \delta x_{23}^*]$. This section presents some numerical

simulation results to show the performance of the control strategy.

The physical parameters of the model are set to be the parameters of a proposed 1-D hover track test bed and are used to test the control algorithm of the 1-D Coulomb structure stabilization control. The masses of the three spacecraft are $m_1 = m_2 = m_3 = 10$kg, while the desired shape is given as $[\delta x_{12}^*, \delta x_{23}^*] = [4, 4]$m. The separation distances between craft are within 5 meters. Without loss of generality, let the magnitudes of the charges of the spacecraft share a common limit $q_{max} = 5 \times 10^{-5}$C. Let us choose the initial positions and velocities to be:

$$[x_1, x_2, x_3] = [-3, 0, 2]\text{m} \tag{62}$$

$$[\dot{x}_1, \dot{x}_2, \dot{x}_3] = [-0.04, 0, 0.04]\text{m/s} \tag{63}$$

Figure 6 shows the first stage of the control which arrests the relative motion. The two simulation stage results are illustrated separately because the saturated control has a stronger control forces and the relative motion converges much faster than the time needed in the continuous shape control. The parameters of the saturated regulator are $p_1 = p_2 = 1$kg/(C^2·s). The relative distance rates converge to zero in a very short time, and the control charges are always saturated until the distance rates converge. The stability of the control is guaranteed, and if the initial conditions are within the convergence area presented in the last section, then the relative rates will converge to zero.

Figure 7 illustrates the simulation results of the second stage, continuous formation shape control. The parameters of this control are

$$[K] = \begin{bmatrix} 3.6 & 0 \\ 0 & 1.8 \end{bmatrix} \text{kgm/s}^2, \; [P] = \begin{bmatrix} 14.4 & 0 \\ 0 & 7.2 \end{bmatrix} \text{kgm/s} \tag{64}$$

The values of matrices $[K]$ and $[P]$ are chosen to balance between the overshooting and the response speed. Figure 7(a) and (b) show the process of the Coulomb structure to converge to the desired shape. Figure 7(c) and (d) are the charge histories under different conditions. The chattering issue of the charges is nontrivial in the control process. As mentioned before in the formation shape control section, the chattering effect is partly due to the switching between two possible values of the variable τ. The parameter $\alpha \leq 1$ has been introduced to buffer the switching. With $\alpha = 1$, no buffer is acting on the system. When $0 < \alpha < 1$, the buffer is taking effect. Comparing Figure 7(c) and (d), it can be seen that when $\alpha = 0.7$, the chattering effect is reduced to some extent. Though the buffer can not totally eliminate the chattering, the benefit is that this approach doesn't influence the dynamics of the system. This is because any value of the variable τ results in a vector that is within the null space of the input matrix of the control.

VI. CONCLUSION

A two-stage stable charge feedback control strategy is developed to shape the configuration of the 1-D restricted Coulomb structure. The first stage intends to arrest the relative motion
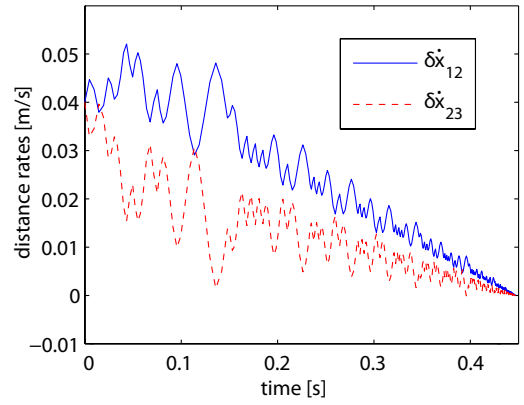
(a) Separation distance rates.
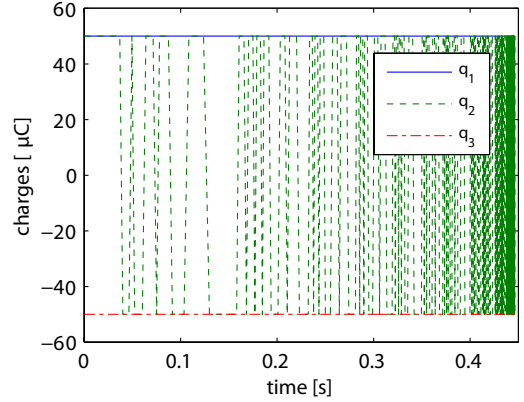
(b) Control charges' histories.

Fig. 6. Numerical Simulation Results of Stage I: Relative Motion Regulation.

of the formation. A globally stable, but not asymptotically stable saturated control is designed using Lyapunov's direct method. Varying the value of a positive definite matrix used in designing the Lyapunov function rate guarantees real charge solutions. The analytical criterion for a stabilizable symmetric motion is obtained by evaluating the total energy level of the system. For general cases, the convergence areas of the initial states for stabilizable motions are illustrated numerically. The second stage is a continuous formation shape control. It is used to control the shape of the Coulomb structure to a certain desired configuration. The control is also designed using Lyapunov's method. A minimum charge search routine in the null space of the input matrix is used to solve the control charge implementability problem. The search routine not only makes the charge control law physically implementable, but also results in minimum control charges at every instance. Numerical simulations verify the effectiveness of the control strategy.

This paper stands for a good foundation for the future general 3D Coulomb structure control. 3D Coulomb structure control would be much more complicated because the angular momentum of the three spacecraft system might make the shape control never converge, but with a certain boundary.
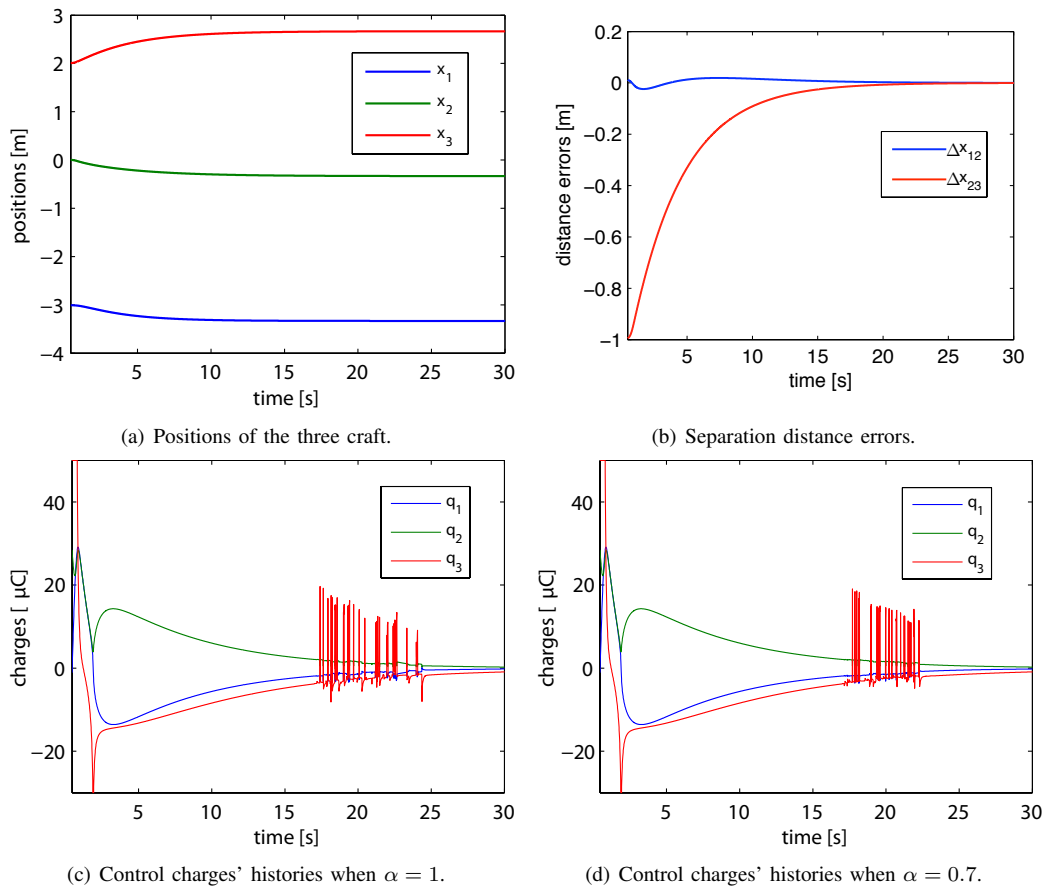
(a) Positions of the three craft.

(b) Separation distance errors.

(c) Control charges' histories when $\alpha = 1$.

(d) Control charges' histories when $\alpha = 0.7$.

Fig. 7.   Numerical Simulation Results of Stage II: Formation Shape Control.

REFERENCES

[1] Lyon B. King, Gordon G. Parker, and Satwik Deshmukh et al. Spacecraft formation flying using inter-vehicle coulomb forces. *Tech. rep., NASA/NIAC*, January 2002.

[2] Edmund M. C. Kong and Daniel W. Kwon et al. Electromagnetic formation flight for multisatellite arrays. *Journal of Spacecraft and Rockets*, 41(4), July-August 2004.

[3] Lyon B. King, Gordon G. Parker, Satwik Deshmukh, and Jer-Hong Chong. A study of inter-spacecraft coulomb forces and implications for formation flying. *38th AIAA/ASME/SAE/ASEE Joint Propulsion Conference Exhibit, Indianapolis, Indiana*, July 2002.

[4] Hyunsik Joe, Hanspeter Schaub, and Gordon G. Parker. Formation dynamics of coulomb satellites. *6th International Conference on Dynamics and Control of Systems and Structures in Space*, July 18-22 2004.

[5] Gordon G. Parker, Chris E. Passerello, and Hanspeter Schaub. Static formation control using interspacecraft coulomb forces. *2nd International Symposium on Formation Flying Missions and Technologies*, Sept. 14-16 2004.

[6] Hanspeter Schaub and Mischa Kim. Differential orbit element constraints for coulomb satellite formations. *Astrodynamics Specialist Conference*, Aug. 16–19 2004.

[7] Arun Natarajan and Hanspeter Schaub. Linear dynamics and stability analysis of a coulomb tether formation. *AIAA Journal of Guidance, Control, and Dynamics*, 29(4):831–839, July–Aug. 2006.

[8] Arun Natarajan, Hanspeter Schaub, and Gordon G. Parker. Reconfiguration of a nadir-pointing 2-craft coulomb tether. *Journal of British Interplanetary Society*, 60(6):209–218, June 2007.

[9] Arun Natarajan and Hanspeter Schaub. Hybrid conrol of orbit normal and along-track 2-craft coulomb tethers. In *AAS Space Flight Mechanics Meeting*, Sedona, AZ, Jan. 28–Feb. 1 2007. Paper AAS 07–193.

[10] Islam I. Hussein and Hanspeter Schaub. Invariant shape solutions of the spinning three craft coulomb tether problem. *Celestial Mechanics and Dynamical Astronomy*, 96(2):137–157, Oct. 2006.

[11] Hanspeter Schaub and Islam I. Hussein. Stability and reconfiguration analysis of a circulary spinning 2-craft coulomb tether. In *IEEE Aerospace Conference*, Big Sky, MT, March 3–10 2007.

[12] Islam I. Hussein and Hanspeter Schaub. Stability and control of relative equilibria for the three-spacecraft coulomb tether problem. In *AAS/AIAA Astrodynamics Specialists Conference*, Mackinac Island, MI, Aug. 19–23 2007. Paper AAS 07–269.

[13] John Berryman and Hanspeter Schaub. Analytical charge analysis for 2- and 3-craft coulomb formations. In *AAS/AIAA Astrodynamics Specialists Conference*, Lake Tahoe, CA, Aug. 7–11, 2005 2005. Paper No. 05-278.

[14] Rush D. Robinett, Gordon G. Parker, Hanspeter Schaub, and John L. Junkins. Lyapunov optimal saturated control for nonlinear systems. *AIAA Journal of Guidance, Control, and Dynamics*, 20(6):1083–1088, Nov.–Dec. 1997.

[15] Shuquan Wang and Hanspeter Schaub. Spacecraft collision avoidance using coulomb forces with separation distance feedback. In *17th AAS/AIAA Space Flight Mechanics Meeting*, Sedona, Arizona, January28-February 1 2007. AAS/AIAA.
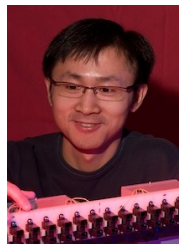
Shuquan Wang Shuquan Wang is a PhD candidate in the Aerospace Engineering Sciences department at the University of Colorado at Boulder, CO. His major research area is Coulomb formation flying (CFF). He has been working on 3-spacecraft Coulomb structure control and 2-spacecraft collision avoidance problem. He got his Master's degree from Chinese Academy of Sciences, with the thesis titled "Adaptive Fuzzy Logic Control For Satellite Attitude Control".

Hanspeter Schaub Dr. Schaub is an associate professor and an H. Joseph Smead Fellow of the Aerospace Engineering Sciences department at the University of Colorado at Boulder. He is an associate fellow of AIAA and member of AAS. His 13 years of professional interests are in nonlinear dynamics and control applications, with a special emphasis on astrodynamics. He has performed research in spacecraft attitude and control, exploiting nonlinear dynamics of control moment gyros to avoid classical CMG singularities, as well as extensive research in spacecraft formation flying dynamics and control problems. His current interests include charged relative motion dynamics and control, as well as visual servoing of autonomous vehicles. Dr. Schaub's prior work experience includes 4 years at the Sandia National Labs Intelligent Systems and Robotics Center (ISRC), and 4 years at the Virginia Tech aerospace and ocean engineering department as an assistant professor. He has authored about 40 peer reviewed papers, presented 60 conference papers, published a text book on analytical mechanics of space systems, and holds a patent on a noncontact position and orientation measurement system.